Bubble Shapes in a Liquid-Filled Rotating Container Under Low Gravity

R. J. Hung*
University of Alabama, Huntsville, Alabama
and
F. W. Leslie†
NASA Marshall Space Flight Center, Huntsville, Alabama

The effect of surface tension on steady-state rotating fluids in a low-gravity environment is studied. All values of the physical parameters used in the present calculations, except in the low-gravity environments, are based on the measurements carried out by Leslie[1] in the low-gravity environment of a free-falling aircraft. The profile of the interface of two fluids is derived from Laplace's equation relating pressure drop across an interface to the radii of curvature that has been applied to a low-gravity rotating bubble that contacts the container boundary. The interface shape depends on the ratio of gravity to surface-tension forces, the ratio of centrifugal to surface tension forces, the contact radius of the interface to the boundary, and the contact angle. The shape of the bubble is symmetric about its equator in a zero-gravity environment. This symmetry disappears and gradually shifts to parabolic profiles as the gravity environment becomes nonzero. The location of the maximum radius of the bubble moves upward from the center of the depth toward the top boundary of the cylinder as gravity increases. The contact radius of interface to the boundary r_o at the top side of cylinder increases, and r_o at the bottom side of the cylinder decreases as the gravity environment increases from zero to 1 g.

Introduction

A CYLINDRICAL container partially filled with a Newtonian fluid of constant density, rotating about its axis of symmetry, under a low-gravity environment, is considered in the present study. Knowledge of this internal flow is needed to design gun-launched projectiles that carry smoke/incendiary agents or chemical payloads. It is also relevant to liquid propellant in spacecraft fuel-tank design in which sloshing and a series of bubbles are created during the space flight. Liquid payloads enhance spin decay of projectiles,[2,3] and their presence can produce flight dynamic instabilities as a result of resonance between the projectile nutational motion and inertial oscillations in the rotating liquid.[4] From a computational viewpoint, this problem is instructive because it is an example of a class of internal flow problems for which computational experiments can uncover details of the flow that can not be easily visualized or measured experimentally.[5]

Surface tension plays an important role in a large variety of fluid flows. These range from rather small-scale phenomena, such as the breakup or coalescence of raindrops, to large-scale flows, like the motion of liquid propellant in a space vehicle under low-gravity conditions. Free surface shapes of liquids also play a key role in spacecraft fuel-tank design and in fluid management systems. In some spacecraft fuel-tank applications, propellant slosh and distribution are controlled with the use of internal baffles that come into contact with the free surface. If the liquid is to be held using capillary forces, in addition to the low-gravity forces, the baffle spacing must be small enough to overcome the fluid's inertial forces during small accelerations brought about by thruster firings, crew motion, etc. The problem can be complicated by rotation of the container. In any case, in order to manage the liquid, distribution of the fluid including its interface shape must be determined.

Rosenthal[6] computed the shapes of rotating bubbles in the absence of gravity. He found that for large rotation rates the aspect ratio of a free bubble is proportional to the square of the rotation rate. Chandrasekhar[7] examined the stability of a rotating liquid drop and derived the analytical formula for the equilibrium shapes based on Laplace's equation for the pressure drop across the interface. By using a spherical coordinate system, Busse[8] determined the equilibrium shape for a rotating liquid drop in terms of a Legendre function expansion. Tieu et al.[9] obtained solutions for motion and interface shape of a two-fluid system contained in an oscillating vertical cylinder. Using a domain perturbation approach, they obtained first- and second-order solutions in a 1 g environment. Experimental results were in qualitative agreement with their theoretical predictions.

Recently, Leslie[1] performed a series of measurements on rotating equilibrium free-surface shapes in the low-gravity environment of a free-falling aircraft (KC-135). The apparatus consisted of a Plexiglas cylinder with different depths. The cylinder was partially filled with ethanol, chosen because 1) its surface tension is relatively high (2.28×10^{-2} N/m with air at 1 atm and 20°C); 2) the value of surface tension is not very sensitive to low levels of contamination; 3) its contact line with the container does not stick; and 4) its contact angle is close to zero. The cylinder was fastened to a turntable that rotated about the cylinder's axis. After the cylinder was filled with ethanol, a prescribed amount was removed to establish the bubble volume.

Leslie was able to measure and to compute numerically the bubble shapes at various ratios of centrifugal force to surface tension force in 2-, 4-, and 6.3-cm-deep cylinders in the low-gravity environment. The results show excellent agreement between model computation and measurements. This paper extends his work to rotating free surfaces influenced by gravity. The special case of zero gravity is used to validate the computations by comparing them with Leslie's results.[1]

Received Oct. 23, 1986; presented as Paper 87-0616 at the AIAA 25th Aerospace Sciences Meeting, Reno, NV, Jan. 12-15, 1987; revision submitted July 16, 1987.

*Professor, Mechanical Engineering Department. Associate Fellow AIAA.

†Research Scientist, Chief of Fluid Dynamics Branch. Member AIAA.

Mathematical Model

At the surface of two fluids, pressure discontinuity is governed by the Laplace's formula

$$P^i - P^o = \sigma \underset{\sim}{\nabla} \cdot \hat{n}_o \tag{1}$$

where P^i denotes pressure inside the bubble, P^o the pressure outside the bubble, σ the coefficient of surface tension, and $\hat{n}_o$ the unit normal vector pointing outward from the surface.

In general, P^i and P^o are determined from the full set of Navier-Stokes equations. For the special case of a steady-state rotating fluid, with the assumption of axial symmetry, P^i and P^o can be easily determined analytically from the Navier-Stokes equations. The solutions in cylindrical coordinates are given by

$$P^i = P^i_o + 1/2\ \rho_i \omega^2 r^2 - \rho_i g z \tag{2}$$

$$P^o = P^o_o + 1/2\ \rho_o \omega^2 r^2 - \rho_o g z \tag{3}$$

where ρ is density of fluid, ω the rotation rate of the fluid, g the gravitational acceleration; and subscripts i and o denote physical parameters inside and outside the interface, respectively.

For the case of axial symmetry, the gradient of $\hat{n}_o$ can be further written as

$$\underset{\sim}{\nabla} \cdot \hat{n}_o = R_1^{-1} + R_2^{-1} \tag{4}$$

where

$$R_1^{-1} = \frac{d^2z}{dr^2}\left[1 + \left(\frac{dz}{dr}\right)^2\right]^{-3/2} \tag{5a}$$

$$R_2^{-1} = \frac{dz}{dr} r^{-1}\left[1 + \left(\frac{dz}{dr}\right)^2\right]^{-1/2} \tag{5b}$$

Now, let the profile of the interface be given by $z = f(r)$, and define the following parameters:

$$\phi = \frac{dz}{dr} = \frac{df}{dr} \quad \text{and} \quad \phi' = \frac{d\phi}{dr} = \frac{d^2z}{dr^2}$$

Equation (4) can be rewritten in the form

$$\underset{\sim}{\nabla} \cdot \hat{n}_o = -\frac{1}{r}\frac{d}{dr}\left[\frac{r\phi}{(1+\phi^2)^{1/2}}\right] \tag{6}$$

Substituting Eqs. (2-4) in Eq. (1) leads to

$$P_o r + \frac{1}{2}\rho\omega^2 r^3 - \rho g z r = -\sigma \frac{d}{dr}\left[\frac{r\phi}{(1+\phi^2)^{1/2}}\right] \tag{7}$$

where $P_o = P^i_o - P^o_o$ and $\rho = \rho_i - \rho_o$. The boundary condition for Eq. (7) is

$$\phi\Big|_{r=r_o} = -\tan\theta \tag{8}$$

where θ is contact angle between the horizontal boundary of fluid and the outer wall (see Fig. 1), and r_o the radius of the bubble that intersects the top of the cylinder at height L.

Integrating Eq. (4) leads to

$$\frac{1}{2}P_o r^2 + \frac{1}{8}\rho\omega^2 r^4 - \rho g \int rz\,dr = -\frac{\sigma r\phi}{(1+\phi^2)^{1/2}} + C \tag{9}$$

Constant C can be determined by using Eq. (8) and is given by

$$C = \frac{1}{2}P_o r_o^2 + \frac{1}{8}\rho\omega^2 r_o^4 - \rho g \int rz\,dr\Big|_{r=r_o} - \sigma r_o \sin\theta \tag{10}$$

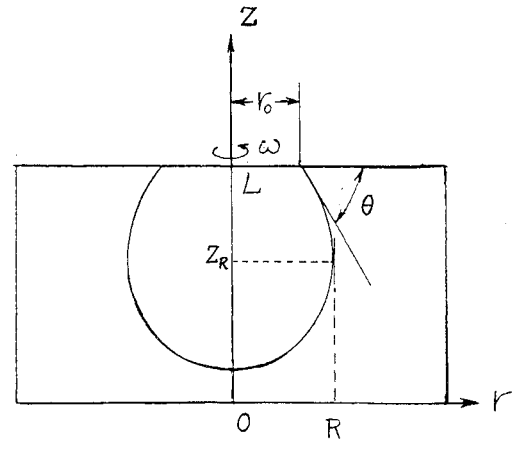

Fig. 1 Definition of the cylindrical coordinate systems for the bubble and rotating fluids used for the analytical model.

The value of P_o can be evaluated at $r = R$, the maximum radius of the bubble where $\phi \to -\infty$ (see Fig. 1 for description). This is

$$P_o = -\frac{2}{R\left[1 - \left(\frac{r_o}{R}\right)^2\right]}\left\{\frac{1}{8}\rho\omega^2 R^3\left[1 - \left(\frac{r_o}{R}\right)^4\right] - \frac{\rho g}{R}\int_{r_o}^{R} rz\,dr + \sigma\left(1 + \frac{r_o}{R}\sin\theta\right)\right\} \tag{11}$$

Substituting Eqs. (10) and (11) in Eq. (9) leads to

$$A = -\frac{\sigma r\phi}{(1+\phi^2)^{1/2}} \tag{12}$$

where

$$A = -\frac{1}{R\left[1 - \left(\frac{r_o}{R}\right)^2\right]}\left\{\frac{1}{8}\rho\omega^2 R^3\left[1 - \left(\frac{r_o}{R}\right)^4\right] - \frac{\rho g}{R}\int_{r_o}^{R} rz\,dr + \sigma\left(1 + \frac{r_o}{R}\sin\theta\right)\right\}\cdot(r^2 - r_o^2) + \frac{1}{8}\rho\omega^2(r^4 - r_o^4) - \rho g\int_{r_o}^{r} rz\,dr + \sigma r_o \sin\theta$$

Solving for ϕ from Eq. (12) one obtains

$$\phi = \frac{\psi}{(1-\psi^2)^{1/2}} \tag{13}$$

where

$$\psi = \frac{A}{\sigma r} = \frac{1}{\hat{r}}\left\{\frac{\hat{r}_o^2 - \hat{r}^2}{1 - \hat{r}_o^2}\left[1 + \hat{r}_o\sin\theta + F(1 - \hat{r}_o^4) - \frac{G}{R^3}\int_{r_o}^{R} rz\,dr\right] + F(\hat{r}^4 - \hat{r}_o^4) - \frac{G}{R^3}\int_{r_o}^{r} rz\,dr + \hat{r}_o\sin\theta\right\} \tag{14}$$

$$\hat{r} = \frac{r}{R} \tag{15}$$

$$\hat{r}_o = \frac{r_o}{R} \tag{16}$$

$$F = \frac{\rho\omega^2 R^3}{8\sigma} = \frac{\text{centrifugal force}}{\text{surface tension force}} \tag{17}$$

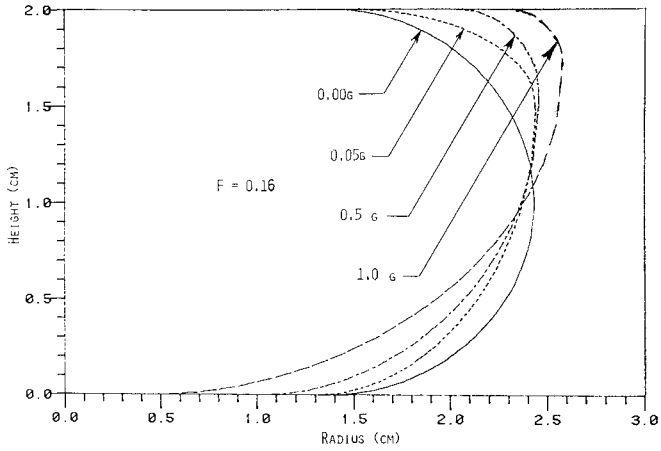

Fig. 2 Computed profiles of the bubble in a 2-cm-deep cylinder for $F = 0.6$ in the gravity environments of 0.00, 0.05, 0.5, and 1.0 g.

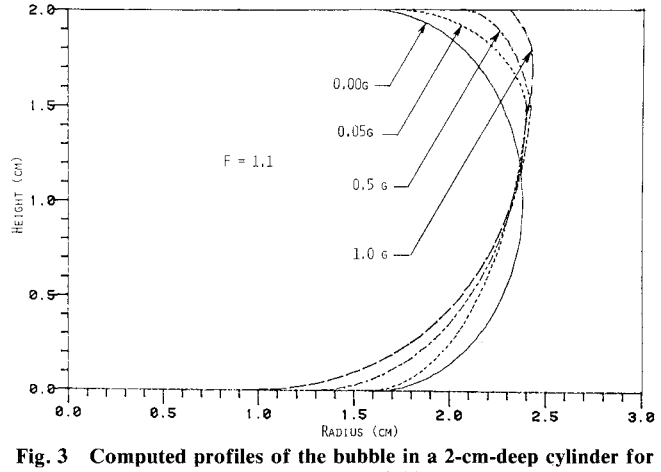

Fig. 3 Computed profiles of the bubble in a 2-cm-deep cylinder for $F = 1.1$ in the gravity environments of 0.00, 0.05, 0.5, and 1.0 g.

$$G = \frac{\rho g R^2}{\sigma} = \frac{\text{gravity force}}{\text{surface tension force}} \tag{18}$$

Since $\phi = dz/dr$, profile of the interface becomes

$$\frac{z}{R} = f(\hat{r}) = \int_{\hat{r}_o}^{\hat{r}} \frac{\psi}{(1-\psi^2)^{1/2}}\, d\hat{r} \tag{19}$$

For the special case of zero-gravity ($G \to 0$), Eq. (14) reduces to the equation obtained by Leslie.[1] In addition, for the case of a free bubble not contacting the top and/or bottom of the cylinder ($r_o = 0$) and zero contact angle ($\theta = 0$), Eq. (19) is equivalent to Chandrasekhar's equation for the shape of a rotating free drop. Also, for the additional case of zero centrifugal force ($F = 0$), Eq. (19) represents a sphere.

Numerical Calculation of the Bubble Shapes

The present study examines rotating bubbles that may intersect the top and bottom boundaries. Numerical calculations were performed for various values of the parameters F and G as well as the vapor volumes from the experiments. In each set of the experiments accomplished for the profiles of the rotating bubbles, different gravity environments of 0, 0.05, 0.5, and 1 g have been computed. The calculations were initiated with an estimate of the bubble shape for computing the integral term in Eq. (14). A number of iterations were made to minimize the difference between the trial profile of the bubble shape in the integration of $\int rz\,dr$ in Eq. (14), and the final profile of the bubble shape obtained from the integration of Eq. (19). After the integration was complete, the measured volume and the computed volume were compared.

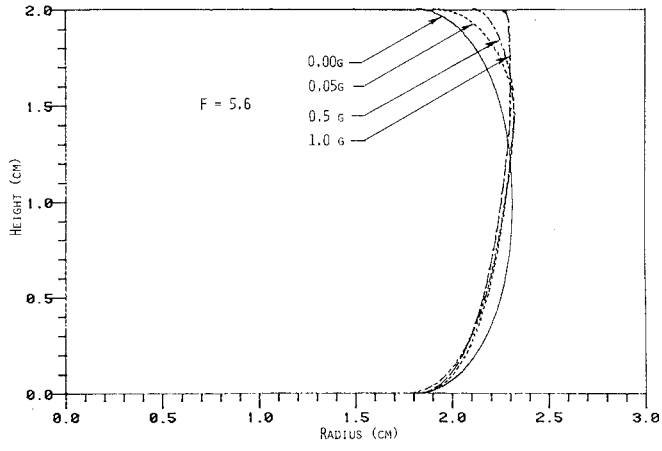

Fig. 4 Computed profiles of the bubble in a 2-cm-deep cylinder for $F = 5.6$ in the gravity environments of 0.00, 0.05, 0.5, and 1.0 g.

At the location of maximum radius of the bubble, the value of Z becomes

$$z\Big|_{\hat{r}=1} = z\Big|_{\phi \to -\infty} = z_R(\hat{r}=1) \tag{20}$$

We can divide the region of calculation in Eq. (13) and region of integration in Eq. (19) into the following two regions:

$$\phi < 0 \quad \text{for} \quad L \geq z > z_R \tag{21}$$

and

$$\phi > 0 \quad \text{for} \quad z_R > z \geq 0 \tag{22}$$

In other words, the calculation of bubble shape is divided into two regions, one for the shape above the maximum radius of the bubble, and the other for its shape below the maximum radius of the bubble. In doing so, the difficulty of showing two values of z for each value of r for solving Eqs. (13) and (19) can be avoided.

Figures 2–4 show the comparison of the calculated interface profiles for small, moderate, and large values of F in various gravity environments, respectively. The cylinder depths are all 2 cm. The profiles in Fig. 2 are for low-rotation cases that are dominated by capillary forces. The interface surface is nearly spherical, and the maximum radius of the bubble located at the half depth of the cylinder ($z = 1/2$) for the case in the zero-gravity environment is in good agreement with the result obtained by Leslie.[1] As the gravity force increases from zero gravity the profile quickly deviates from spherical. The location of the maximum radius of the bubble moves upward from the center of the depth toward the top boundary of the cylinder, while $\hat{r}_o$ at the topside of the cylinder increases, and $\hat{r}_o$ at the bottom side of the cylinder decreases.

Figure 3 shows the profiles for a moderate value of F. Here the capillary and centrifugal forces are about equal and the interface has become more prolate. It may be seen that the value of $\hat{r}_o$ at the topside of the cylinder has increased, while that at the bottom side of the cylinder has decreased when the gravity environment is greater than zero. The qualitative change of the free surface shape with the addition of gravity is much like that in Fig. 2. Similarly, Fig. 4 shows the profiles of the bubble for a large value of F. The interface here is dominated by the centrifugal force and the surface is more flat and parallel with the rotation axis, except at the top and bottom boundaries, where they are constrained to intersect at the prescribed angle and are influenced by gravity.

Figures 5–7 show interface shapes for a cylinder depth of 4 cm. For a given bubble volume, Leslie's experiments[1] indicated that larger rotation rates are needed in order for the

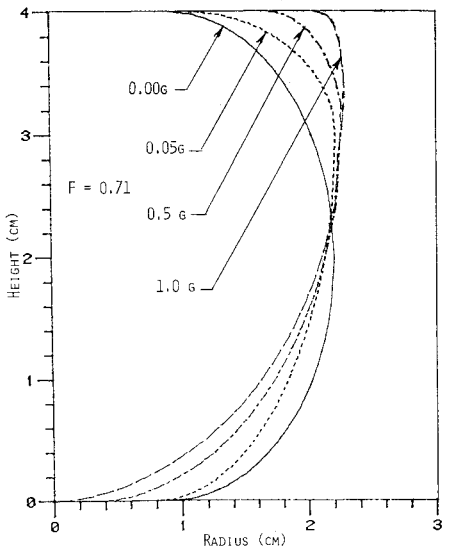

Fig. 5 Computed profiles of the bubble in a 4-cm-deep cylinder for $F = 0.71$ in the gravity environments of 0.00, 0.05, 0.5, and 1.0 g.

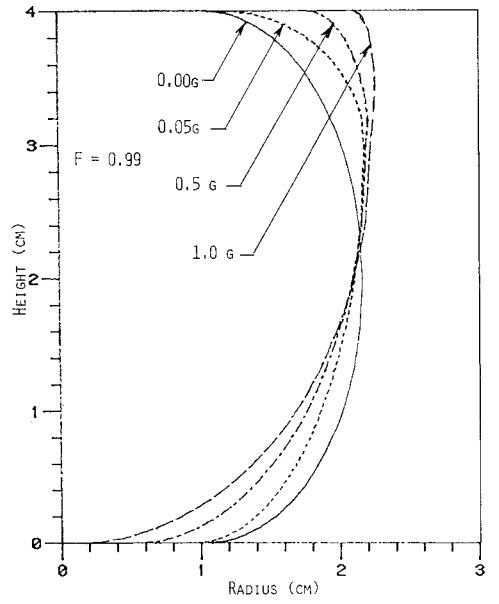

Fig. 6 Computed profiles of the bubble in a 4-cm-deep cylinder for $F = 0.99$ in the gravity environments of 0.00, 0.05, 0.5, and 1.0 g.

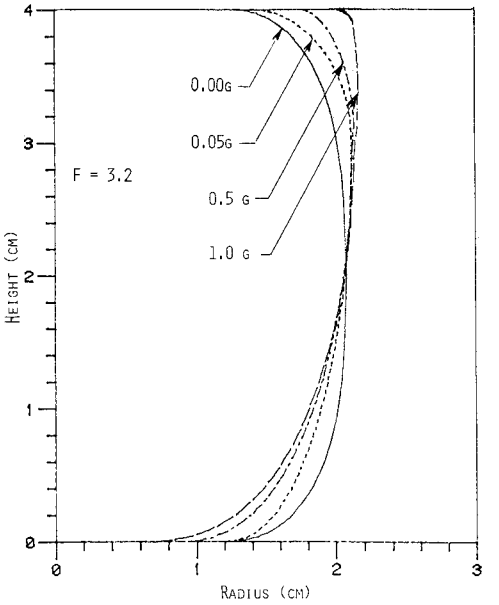

Fig. 7 Computed profiles of the bubble in a 4-cm-deep cylinder for $F = 3.2$ in the gravity environments of 0.00, 0.05, 0.5, and 1.0 g.

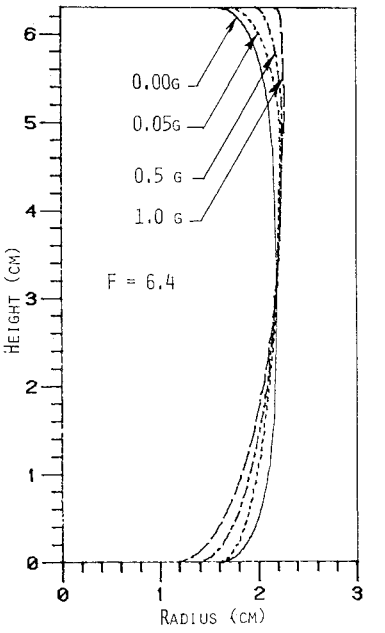

Fig. 8 Computed profiles of the bubble in a 6.3-cm-deep cylinder for $F = 6.4$ in the gravity environments of 0.00, 0.05, 0.5, and 1.0 g.

bubble to contact the top and bottom boundaries, as is also required by the theory. Otherwise, the bubble with a smaller diameter than the cylinder gap meanders along the axis or attaches to the top or bottom boundary. Figure 5 shows a series of profiles for a different gravity environment in which the centrifugal force is less than the capillary force. The experiments indicated this case to be one of the slower relative rotation rates that could stabilize the bubble.[1] These profiles also show that the location of the maximum radius of the bubble moves upward from the center of the depth toward the top boundary of the cylinder, while $\hat{r_o}$ at the topside of the cylinder increases and $\hat{r_o}$ at the bottom side of the cylinder decreases as the gravity environment increases from zero gravity to 1 g. Figure 6 shows profiles in which centrifugal and capillary forces are about equal. The value of F is about the same as for the profiles in Fig. 3. However, $\hat{r_o}$ had to be appropriately decreased for the computation in order for the interface height to match the deeper container. Figure 7 shows interface profiles for $F = 3.2$. Because capillary forces are weak, the interfaces are almost cylindrical except for their contact points with the top and bottom boundaries and the effects of the gravity force that shifts the profiles to be more parabolic. The capillary rise occurs over thinner layers, in the neighborhood of the top and bottom boundaries of the cylinder, in order that the small radius of curvature can generate a sufficient pressure drop to account for the increased hydrostatic contribution.

Finally, Fig. 8 shows the interface profiles for a rotating cylinder of 6.3 cm depth. For a similar ullage volume, larger values of F are required to produce the interfaces with top and bottom boundary contacts. An increase in F produces a more cylindrical bubble. The figure shows the resulting thinner layers, in the neighborhood of top and bottom boundaries, over which the surface tension acts to meet the contact angle requirement. The profiles are also modified by the effect of the gravity force that shifts the profiles to be more parabolic, and the general slope increases as the gravity force changes from 0 to 1 g.

Discussions and Conclusions

The profiles of a rotating interface, given by Eq. (19), are derived from Laplace's equation relating the pressure drop across an interface to the radii of curvature that has been applied to a low-gravity rotating bubble that contacts the container boundary. Solutions to the equation are dependent upon several parameters, namely, G, the ratio of gravity to surface-tension forces; F, the ratio of centrifugal to surface-tension forces; $\hat{r_o}$, the contact radius of the interface to the boundary; and θ, the contact angle. For the cases presented here the contact angle, based on the experiments conducted by Leslie,[1] was nearly zero, which permits a greater range of solutions. The physical parameters used in the numerical calculations are based on experiments performed by Leslie[1] in a free-falling KC-135 aircraft.

For the case of G approaching zero, the bubble is rotating in the zero-gravity environment. Leslie's bubble profile calculations and experiments[1] were in good agreement. The $G = 0$ case presented here also overlaps with Leslie's calculation. As to the cases of G approaching infinity, surface tension is negligible and the profile of the rotating bubble can be easily obtained from Eq. (7) as

$$z = \frac{1}{2g}\omega^2 r^2 + \frac{P_o}{\rho g} \tag{23}$$

This is simply the profile of a parabola. When the surface tension is different from zero there results a thin layer, in the neighborhood of the boundary, over which surface tension acts to meet the contact angle requirement, and creates a pressure drop across an interface to the radii of curvature. The shape of the bubble is symmetric for upper and lower halves of the depth of the cylinder in the zero-gravity environment. As the gravity environment is different from zero, this symmetry disappears and gradually shifts to parabolic profiles. The location of the maximum radius of the bubble moves upward from the center of the depth toward the top boundary of the cylinder, while $\hat{r_o}$ at the topside of the cylinder increases, and $\hat{r_o}$ at the bottom side of the cylinder decreases as the gravity environment increases from zero gravity to 1 g.

The profile of the bubble becomes a sphere when both G and F vanish. For isolated bubbles in a zero-gravity environment, F has a maximum value of ½.[1] A further increase in F causes the bubble to break contact with the axis of rotation. For larger values of F, the bubble becomes more cylindrical, which is modified by gravity effects that shift the profile from cylindrical-like to parabolic and the capillary rise occurs over a thinner layer.

Acknowledgment

R. J. Hung appreciates the support received from the Marshall Space Flight Center through NASA Grant NAG8-035. The help of numerical computation from Y. N. Chiu is also appreciated.

References

[1]Leslie, F.W., "Measurements of Rotating Bubble Shapes in a Low Gravity Environment," *Journal of Fluid Mechanics,* Vol. 161, 1985, pp. 269–279.

[2]Wedemeyer, E.H., "The Unsteady Flow Within a Spinning Cylinder," *Journal of Fluid Mechanics,* Vol. 20, Pt. 3, 1964, pp. 383–399.

[3]Kitchens, C.W. Jr., Gerber, N., and Sedney, R., "Spin Decay of Liquid-Filled Projectiles," *Journal of Spacecraft and Rockets*, Vol. 15, No. 6, Nov.-Dec. 1978, pp. 348–384.

[4]Stewartson, K., "On the Stability of a Spinning Top Containing Liquid," *Journal of Fluid Mechanics,* Vol. 4, 1959, pp. 577–592.

[5]Kitchens, C.W., Jr. "Navier-Stokes Equations for Spin-Up in a Filled Cylinder," *AIAA Journal,* Vol. 18, Aug. 1980, pp. 929–934.

[6]Rosenthal, D.K., "The Shape and Stability of a Bubble at the Axis of a Rotating Liquid," *Journal of Fluid Mechanics,* Vol. 12, 1962, pp. 358–366.

[7]Chandrasekhar, F.R.S., "The Stability of a Rotating Liquid Drop," *Proceedings of the Royal Society of London,* Ser. A, Vol. 286, 1965, pp. 1–26.

[8]Busse, F.H., "Oscillations of a Rotating Liquid Drop," *Journal of Fluid Mechanics,* Vol. 142, 1984, pp. 1–8.

[9]Tieu, H.A., Joseph, D.D., and Beavers, G.S., "Interfacial Shapes Between Two Superimposed Rotating Simple Fluids," *Journal of Fluid Mechanics,* Vol. 145, 1984, pp. 11–70.